CFD simulation of wave impact on a semisubmersible

van der Plas, P.; Veldman, A. E. P.

CFD SIMULATION OF WAVE IMPACT ON A SEMI-SUBMERSIBLE: A NUMERICAL CASE STUDY

P. van der Plas, A.E.P. Veldman
Johan Bernoulli Institute of Mathematics, University of Groningen
Nijenborgh 9, 9747AG Groningen
P.van.der.Plas@rug.nl, A.E.P.Veldman@rug.nl

ABSTRACT: The CFD solver is validated for regular waves impacting a semi-submersible structure. Due to the sensitivity and uncertainties of the experiments in the test basin and sensitivity of the CFD simulations, small variations can introduce significant differences between individual wave periods which complicates the interpretation of the results. In this paper we investigate a statistical approach to comparing CFD results with experiment in order to get a better comparison and to acquire more insight in grid convergence behavior.

1. INTRODUCTION

In offshore applications, extreme events of wave impact on rigid and floating structures are of high interest. The present case study investigates the application of CFD to the simulation of wave impact on a semi-submersible [1, 2]. Various regular waves are considered, of which the properties are only known within a given uncertainty range. Small variations in the incoming wave can cause large differences in the measured impact forces on the structure. This presents a complicating factor in interpreting the CFD results. In a similar fashion, small changes in the simulation setup can cause seemingly disproportionate differences in the solution if interpreted in a deterministic sense. The variation observed in the experimental measurement poses several challenges. Firstly, the experiment has to be reconstructed in the numerical simulation. A representative wave is constructed by means of averaging of the experiment data [3]. Secondly, given the variation of the flow conditions around the semi-submersible in the test basin, a deterministic interpretation of the numerical results is of limited value. In the current study the deterministic comparison is complemented by a statistical approach to assess the average and variation of the impact forces. The statistical approach is also applied to investigate grid convergence behaviour.

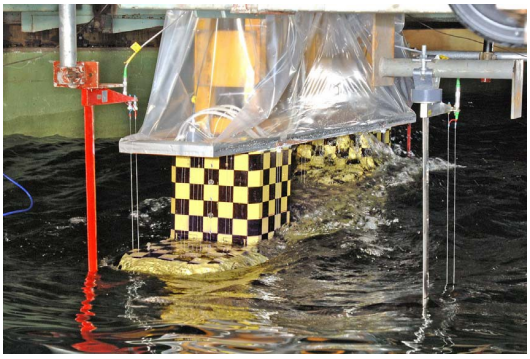

Figure 1: Photo snapshot of wave impact in the semi-submersible model experiment performed at MARIN, courtesy: "SafeFLOW" project

2. PROBLEM DESCRIPTION

In this paper we consider the simulation of wave run-up on a “semi-submersible" offshore structure. A semi-submersible is a special marine vessel used in a number of specific offshore situations such as offshore drilling rigs, safety vessels, oil production platforms, and heavy lift cranes. They are designed with good stability and seakeeping characteristics. Semi-submersibles generally show far less motions in waves than normal ships, making them especially suitable for tasks with very strict motion requirements. Since semi-submersibles are not very mobile, they are designed to withstand severe wheather conditions such as strong winds and extreme wave impact. To guarantee safety conditions and to predict the effects on the structural integrity of the floating object, it is crucial to obtain accurate and reliable predictions of wave loads. In particular the columns and the deck are of interest.

As part of the ComFLOW-2 project, wave run-up model experiments were performed at the Maritime Research Institute in the Netherlands (MARIN) for the validation of the numerical methods in ComFLOW [4]. The experiments concentrated on the flow around two columns of the semi-submersible, as shown in fig. 1 In reality a typical semi-submersible is mounted on four (or more) columns. The experiments were performed at a scale of 1 : 50. At full scale, the semi-submersible has a width of approximately 115 meters.

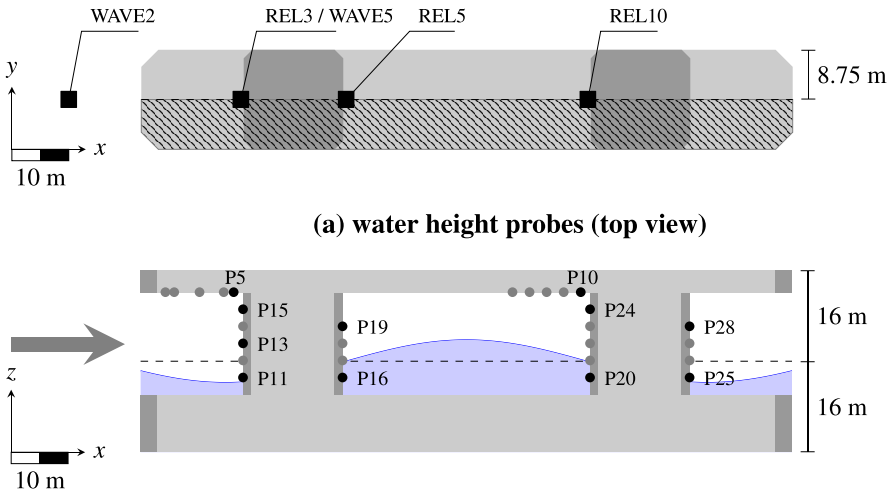

(a) water height probes (top view)

(b) transducers (side view)

Figure 2: Lay-out of the semi-submersible model as used in the experiments performed at MARIN (measurements are given in full scale).

3. THE COMFLOW PACKAGE

ComFLOW is a free-surface flow solver based on a finite-volume discretization of the (compressible) Navier-Stokes equations. The equations are discretized on a staggered Cartesian grid. The fluid transport is implemented by means of a Volume-of-Fluid (VOF) algorithm.

In the past the CFD simulation tool ComFLOW [2] has already been successfully used for wave impact predictions. For accurate prediction of wave run-up and wave loading on offshore structures high resolution is required in the areas of interest. In order to reduce the number of grid points absorbing boundary conditions are used to limit the computational domain. The computational time is further reduced by application of local grid refinement [5] and OpenMP

parallelization. Although the ComFLOW package features both a one-phase incompressible and two-phase compressible model – and certain details of the wave impact may be predicted better by a compressible two-phase fluid model, see [1] – the initial focus of this paper is on the incompressible one-phase fluid solver of ComFLOW.

4. STATISTICAL APPROACH

4.1 Averaging procedure

Simple averaging of the signal $p(t \mod T)$ yields a poor approximation because small phase shifts in the signal can cause details to be filtered out. This problem gets even worse if no good estimate for the period T is available. This particularly becomes an issue for large pressure peaks of short duration.

The problem can be circumvented in two ways:

1. Perform a deterministic approach by selecting a small time frame of several wave periods in which the observed variation is small and compare simulation results and measurements one-on-one. This approach was followed in [6] where the same test case was used to validate the CFD solvers ReFRESCO and ComFLOW.

2. Find an alternative averaging method that accounts for phase shifts in the measured signal and the simulation results.

Both approaches may be equally valid for validation purposes. The large variations in the experiment data are caused by the complexity and sensitivity of the simulated physics on one hand, but also by the sensitivity of the test setup and measurement equipment. Similarly the CFD simulation may show large variations due to round-of errors, reflections from the boundaries of the truncated domain, start-up effects (etc.). These variations may be further magnified by discrete "on-off" mechanisms, such as cell labeling.

When following the deterministic approach, only a few wave periods have to be simulated with CFD. However, afterwards the (variations of the) results have to be interpreted carefully by looking at the entire time traces of the simulation and experiment. For this reason we choose to accept the cost of somewhat longer calculation times and to follow a more statistical approach to the validation of the CFD solver. Instead of directly comparing the simulation results with the actual measurements of the experiment, an averaging approach is used that accounts for the temporal variation in the signals by maximizing the correlation between the individual realizations of the incoming wave.

On itself, the idea of averaging measurements and CFD results is not new. A nice example can be found in [7] where statistics are used to investigate the size distribution of pressure peaks in a sloshing tank. Whereas aligning a single periodically occurring pressure peak is fairly straightforward, In general it is more complicated to design an appropriate synchronization criterion. For this purpose we propose the following averaging procedure:

- Determine an initial guess for the period of the measured signal. In the present test case the period was taken equal to the settings of the wave maker, i.e. $T = 11.0$ [s]. As an alternative, if no guess is available one could inspect the discrete equivalent of the covariance
$$f(\delta t) = \int p(t-\delta t)p(t)\mathrm{d}t.$$

- Divide the signal in n intervals and project them on the time interval $[0,T]$ by taking $p_k := p(t-(k-1)T)$, with $1 \leq k \leq n$.

- Start with the first period as preliminary average $\overline{p}_1 := p_1(t)$. For each following period, subsequently determine the time shift δt_k that maximizes the correlation between the shifted period and the average built up so far. Then calculate the next preliminary average:

$$\overline{p}_k(t) := \left[(k-1)\overline{p}_{k-1} + p_k(\delta t_k)\right]/k.$$

- Finally correct for a possible time shift of the first period, by taking $\overline{p}_n(t+\overline{\delta t})$ with $\overline{\delta t}$ the average of all individual time shifts.

- The observed periodicity is derived by looking at the statistics for $T_k = T + \delta t_{k+1} - \delta t_k$, with $1 \leq k \leq n$.

4.2 Representative incoming wave

Various experimens have been performed involving both regular and irregular incoming waves. For calibration purposes experiments have been performed in an empty basin without semi-submersible. After that, experiments were performed with inclusion of (parts of) the semi-submersible structure. The present work concentrates on the simulation of the test cases with regular incoming waves as listed in table 1.

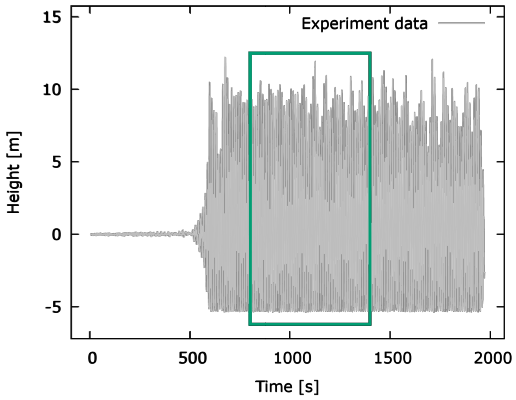

Figure 3: Measurements at water height probe WAVE2

In most practical situations there is no deterministic data available on the incoming waves and one has to resort to statistics. For the experiment discussed in this paper the data is available hence making it possible to opt for a deterministic comparison, for example by selecting a small time frame of the experiment and imposing the corresponding incoming signal at the inflow boundary of the CFD domain. For a regular wave of moderate steepness as is the case here a Stokes-5 fit provides a reasonable representation. Nevertheless the end result depends on several choices that have to be made, such as the time frame to be used, the location of the wave probe(s) for data fitting, et cetera, introducing possible biases. The reconstruction of a representative incoming wave was performed already in [3] and resulted in a Stokes-5 wave with parameters as listed in table 1.

4.3 Time frame of the measurements

The experiment covers a (full scale) time span of approximately 2000 seconds. After approximately 650 seconds the signals demonstrate a periodic character (about 75 periods). Despite

wave	ref.	T [s]	H [m]	λ [m]	H/λ [%]
W15	102004 / 202003	11.01 (11)	14.74 (15)	199.6	7.4

Table 1: Parameters of the incoming Stokes-5 wave as reconstructed from the measurements and as used in the CFD simulations. The originally intended wave period and height are shown between brackets.

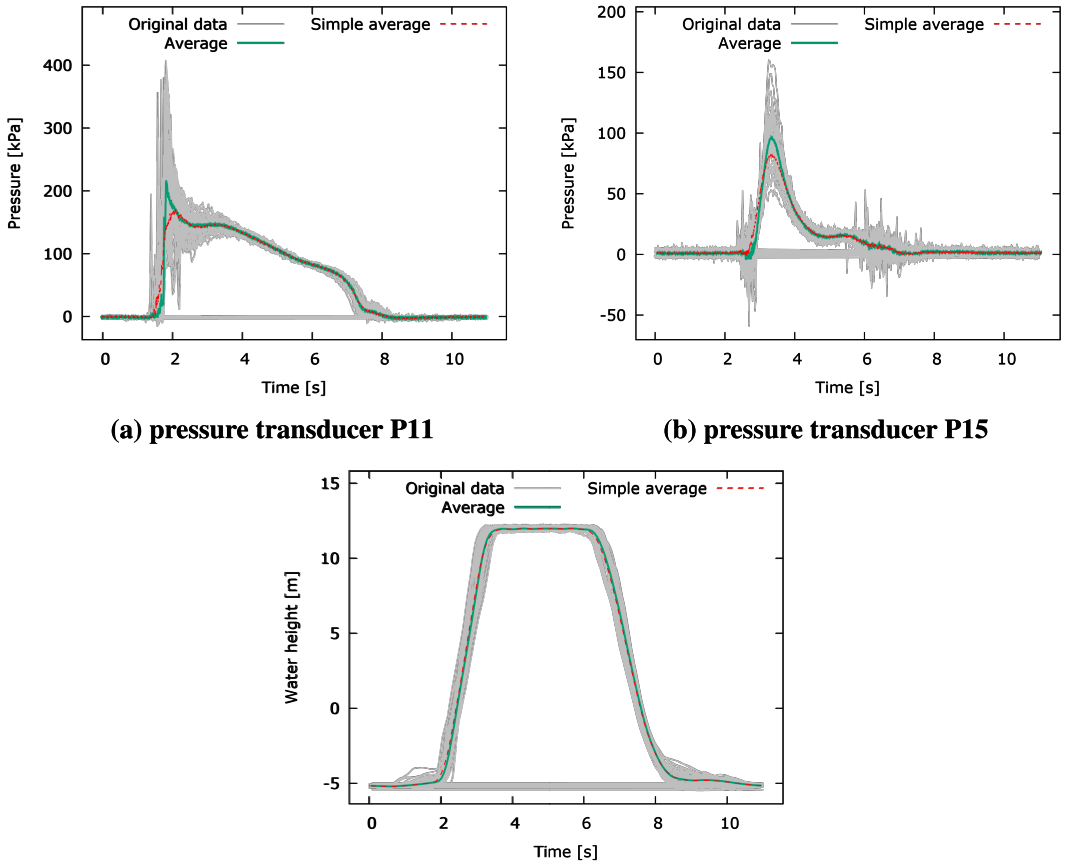

(a) pressure transducer P11

(b) pressure transducer P15

(c) water height probe REL3

Figure 4: Time-averaged and original experiment data of 50 wave periods. The averages are obtained using the method outlined in section 4.1. The orginal data are plotted after applying the best matching time shift.

this periodic character, significant variations can be observed. To exclude start-up effects as well as reflections from the beach at the end of the domain, the validation will be based on the time window $800 \leq t \leq 1400$, covering 54 wave periods. The choice of this time window is based on manual inspection of the measurements: Before and after this time window significant disturbances can be observed in various measurement locations.

In the selected time window an average was calculated of 50 wave periods. The variation in the pressure signal can be significant. E.g. at location "P11", the observed period is 11.0 [s] with a standard deviation of 0.1 [s]. The pressure values for each individual realization differs by approximately 7% to 12% from the averaged signal (normalized to the total area under the curve). In particular peak pressures can be very different upon each impact, which is nicely illustrated in fig. 4b. The variation of the water heights is considerably smaller. The observed

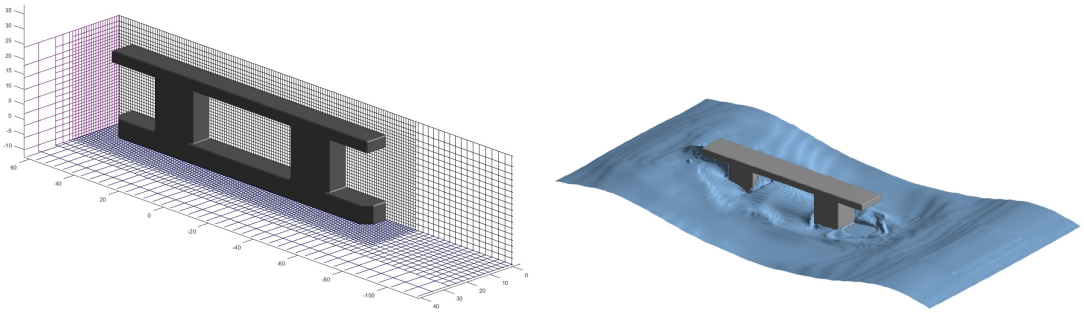

(a) Lay-out of grid "Fine LGR2". **(b) Snapshot of a simulation in ComFLOW.**

Figure 5: Grid lay-out and a snapshot of the numerical simulation on grid "f-LGR2"

wave period is again 11.0 [s] with a standard variation of 0.1 [s]. The total difference with the average water height profile ranges between 3% and 6% as illustrated in fig. 4c. Altogether this shows that the wave period attained in the experiment agree well with the target period.

5. SIMULATION SETUP

Only a small region of several wave lengths is modeled around the semi-submersible, i.e. $-240 \leq x \leq 160$ [m]. At the in- and outflow boundaries a (generating) absorbing boundary condition (GABC) is used [8]. The coefficients for this condition are tuned to the properties of the incoming wave. The sidewards length of the domain is set equal to 200 [m], which corresponds with the (full-scale) width of the test basin. The bottom of the simulation domain is chosen to be at $z = -90$ [m], which is different from the actual (full-scale) depth of 180 [m]. This simplification saves computational time and is not expected to significantly influence the results since wave height and wave length are small compared to the mean water depth.

The semi-submersible is centered around the origin, its mean draft is indicated by the dashed line in fig. 2b. Since the entire problem is symmetrical with respect to the $Y = 0$ plane, a symmetry condition is applied and only one half of the domain is included in the computations as indicated by the dashed region in fig. 2a.

A medium resolution base grid "m-base" is defined with the desired uniform and isotropic resolution d_0 around the semi-submersible. The grid is aligned with the front of the columns of the semi-submersible (and on the fine grid also with the back of the columns), in order to enhance the accuracy of the solution. Two sets of grids are considered, one series at medium resolution $d_0 = 0.5$ [m] and a series at a higher resolution of $d_0 = 1.0$ [m]. The grid is coarsened towards the boundaries of the computational domain by means of stretching and local grid refinement. On simple Cartesian grids the amount of stretching is limited by several requirements. By increasing the resolution around the semi-submersible unnecessary refinement is introduced in the far field, where it is not needed. Furthermore, severe stretching can result in large cell aspect ratios both in the center of stretching and in the far-field, therewith introducing various numerical artifacts. Severe grid stretching, say continuous stretching with factors $r > 1.15$, may lead to instabilities. Furthermore, it was found that large cell aspect ratios, say larger than 4, may negatively affect wave propagation. In particular as the resolution around the semi-submersible becomes larger, this poses a serious restriction on the efficiency of the computational grid, which can only be overcome by means of local grid refinement.

In order to reduce computational time the grid is coarsened in the far field by means of local refinement to obtain the grids as listed in table 2. Figure 5a illustrates a typical refinement

configuration: The grid is mildly coarsened in a strip around the semi-submersible to ensure good resolution of the incoming wave and is only coarsened further in the far-field in Y and Z direction. The coarsest grid ("m-LGR2") has a far-field resolution of $\delta x \approx \lambda/17$; the medium-sized grids ("m-LGR1","m-base","f-LGR2") all have a far-field resolution of $\delta x \approx \lambda/35$, and the finest grid ("f-LGR1") considered in this study has a far-field resolution of $\delta x \approx \lambda/70$. Similarly the vertical far-field grid spacings vary between $\delta z \approx H/5$ to $\delta z \approx H/20$. Since the incoming wave is long-crested, it is possible to be less restrictive on coarsening in the far-field areas in sidewards direction.

	#C	#F	d_0 [m]	#cycles	#iter	#cores	wallclock [h]
m–LGR2	0.28M	0.15M	1.0	11k	0.33M	1	9
m–LGR1	0.40M	0.21M	1.0	11k	0.35M	1	17
m–base	0.66M	0.39M	1.0	11k	0.37M	1	25
f–LGR2	1.3M	0.55M	0.5	17k	1.2M	4	37
f–LGR1	2.1M	0.92M	0.5	17k	1.2M	4	72

Table 2: Overview of the employed grid configurations. "#C" denotes the total number of cells; the computational load is primarily determined by the number of fluid cells, denoted by "#F". The wall clock times are those for the simulations discussed in section 6.2. The columns "#cycles" and "#iter" denote the total number of time steps and linear solver iterations.

6. NUMERICAL RESULTS

The results presented in this section have all been obtained by means of the averaging procedure described in section 4.1. In total a little over 11 wave periods were simulated of which the last 9 were used to obtain average solutions and other statistics. The simulation results were synchronized to the experiment at a single measurement location, in this case being "WAVE2".

6.1 2D wave simulations without semi-submersible

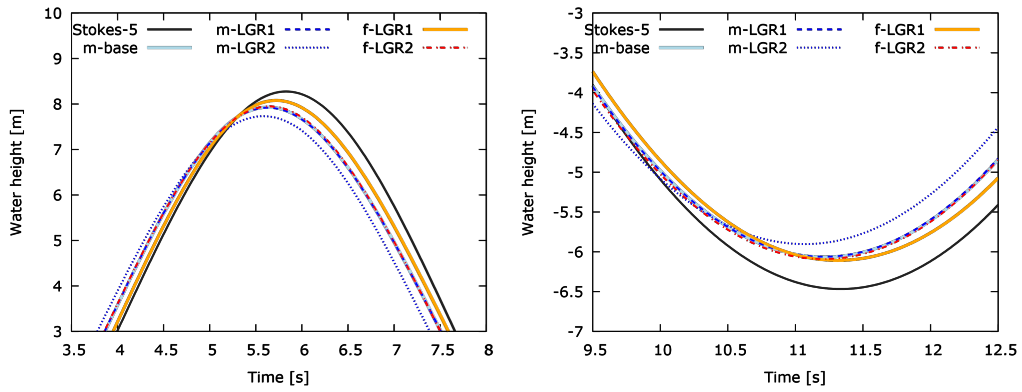

Figure 6: Results for water height probe WAVE5.

Before performing simulations including the semi-submersible structure, the propagation of the incoming wave was analyzed in an empty basin, to make sure that the grid has sufficient resolution in the in- and outflow regions.

In fig. 6 it is seen that the wave profile is predicted equally well on most of the grids. Only on grid “m-LGR2”, the approximation becomes worse. This can be explained by the coarse far-field grid resolution, which leads to more artificial wave damping. Because of its poor quality the grid “m-LGR2” was discarded as serious option for simulation of the actual wave impact.

Also on the finer grids the artificial wave damping still amounts to approximately 2 to 3% of the wave height. The current study was performed using first-order upwind convection and a first-order accurate SLIC-VOF method. Wave damping may be reduced by applying the PLIC-based fluid advection and second-order accurate convection scheme of ComFLOW [8], for the sake of brevity this will be investigated in a follow-up study.

6.2 Simulations with semi-submersible

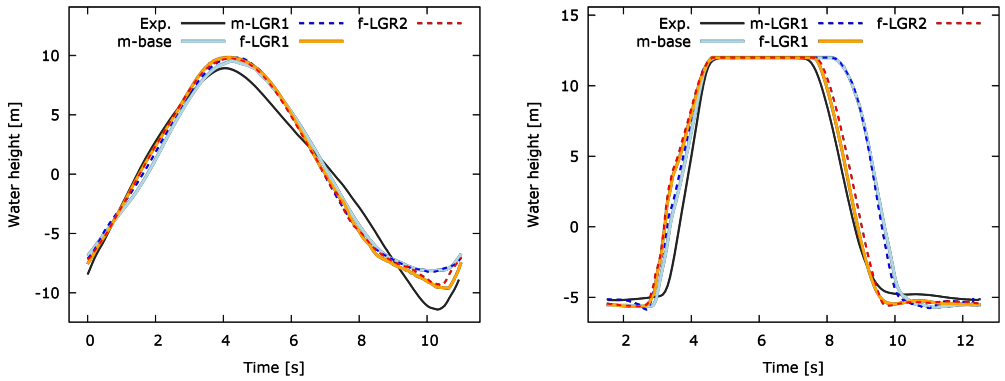

(a) In front, WAVE2

(b) Run-up first column, REL3

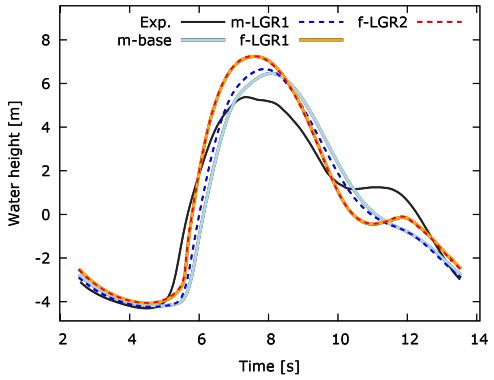

(c) Between the columns, REL5

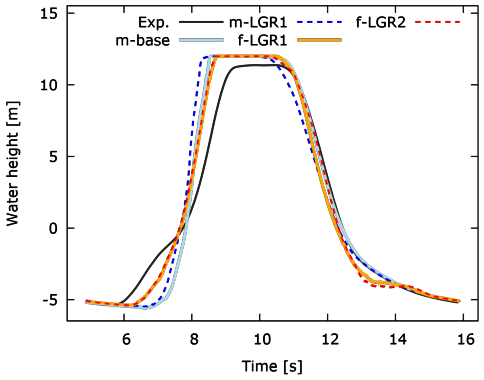

(d) Run-up second column, REL10

Figure 7: Water heights as measured at several locations.

In the experiment a run-up is observed that reaches up to the corners between the columns and the upper deck. The pressure monitors indicate that the water also briefly touches the deck of the structure. This behavior is also observed in the CFD simulations. In general, the water heights around the structure are approximated quite well as is shown in fig. 7. Most of the qualitative details are also captured in the CFD simulation, however at a few points the water heights are somewhat overestimated (see e.g. fig. 7c).

As long as the grid resolution around the semi-submersible and the free surface is kept similar, the quality of the solution is only mildly affected by coarsening in the far-field regions of the grid. Small differences can be observed due to the use of different local grid refinement

configurations, but these are significantly smaller than the differences with the experiment or the differences introduced by refinement around the semi-submersible. This is illustrated in figs. 7 and 8, where the dashed colored lines are mostly on top of the solid lines of the same color. Grid refinement from $d_0 = 1.0$ [m] to $d_0 = 0.5$ [m] causes a clear improvement of the run-up as shown in figs. 7b and 7d. Also the impact pressures on the deck improve considerably as shown in figs. 8e and 8f. Elsewhere the changes due to refinement are of less significance or difficult to interpret. For instance, a sharper impact is registered at monitor point P11, as in the experiment, but it also gets somewhat delayed upon grid refinement.

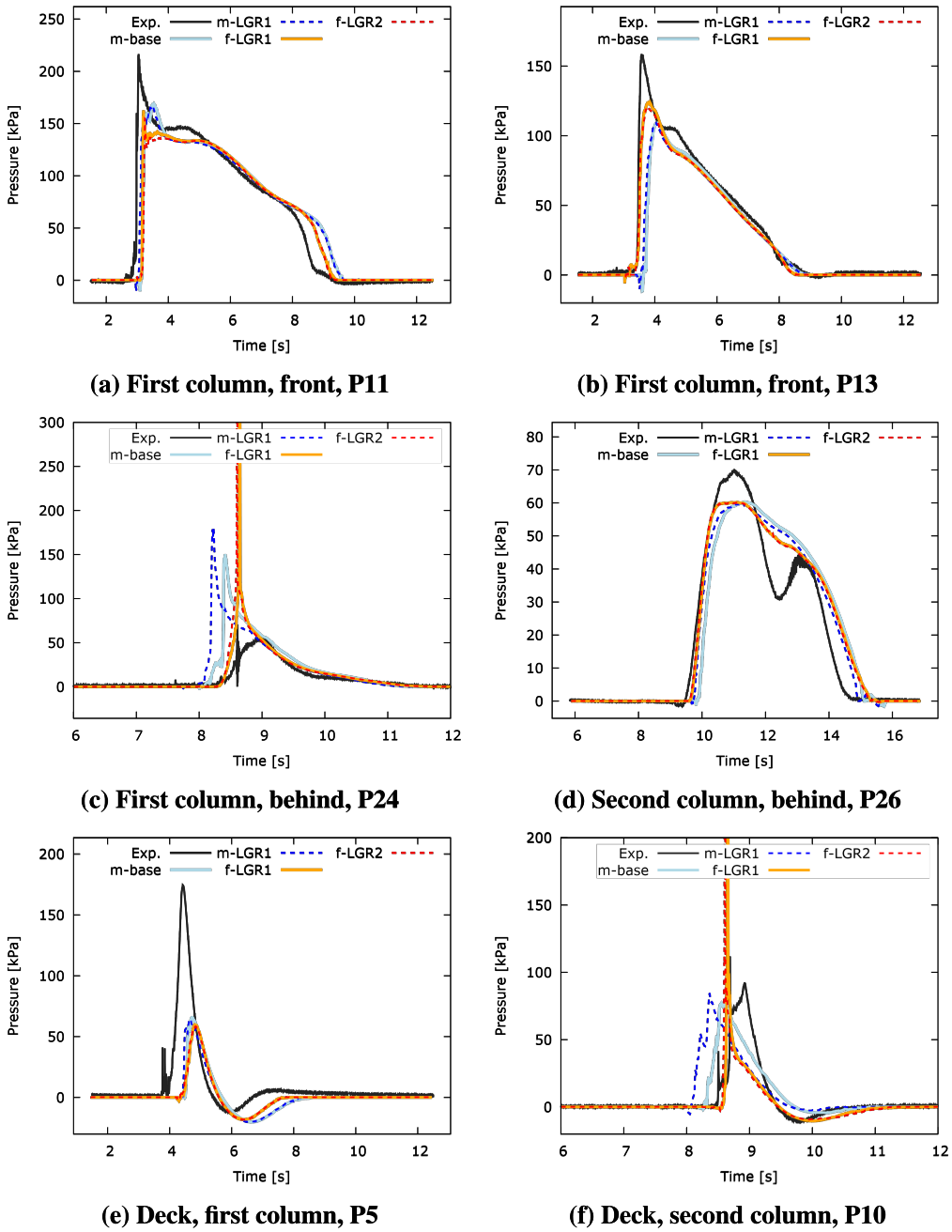

(a) First column, front, P11

(b) First column, front, P13

(c) First column, behind, P24

(d) Second column, behind, P26

(e) Deck, first column, P5

(f) Deck, second column, P10

Figure 8: Pressures as measured at several locations.

7. CONCLUSIONS

A statistical approach was used to validate CFD results with experiment. By means of averaging it was possible to get a better view of grid convergence behavior. Already on coarse grids a relatively accurate prediction can be obtained of the wave impact. Overall, good improvement is observed upon grid refinement. These results suggest that the prediction of run-up along the columns and the impact pressures may improve even further if additional (local) grid refinement is applied or if a higher-order discretization scheme is employed for convection and/or fluid advection. Finally, the average wave period that is observed in the simulations matched well with the one measured in the experiment. In front and behind the semi-submersible the standard deviation is negligible, as in the experiment. However, although the imposed incoming Stokes-5 shows no variation, around the semi-submersible the standard deviation of the wave period is still significantly larger than in the experiment. This is another indication that there is still room for further imroving the accuracy of the CFD calculations.

8. REFERENCES

1. R. Wemmenhove, R. Luppes, A.E.P. Veldman, and T. Bunnik. Numerical simulation of hydrodynamic wave loading by a compressible two-phase flow method. *Comput. Fluids*, 114:218–231, 2015.

2. A.E.P. Veldman, R. Luppes, H.J.L. van der Heiden, P. van der Plas, B. Düz, and R.H.M. Huijsmans. Turbulence modeling, local grid refinement and absorbing boundary conditions for free-surface flow simulations in offshore applications. In *ASME 2014 33rd International Conference on Ocean, Offshore and Arctic Engineering*, 2014.

3. B. Iwanowski, M. Lefranc, and R. Wemmenhove. CFD simulation of wave run-up on a semi-submersible and comparison with experiment. In *ASME 2009 28th International Conference on Ocean, Offshore and Arctic Engineering*, pages 19–29, 2009.

4. R. Wemmenhove. *Numerical simulation of two–phase flow in offshore environments*. PhD thesis, University of Groningen, 2008.

5. P. van der Plas, A.E.P. Veldman, H.J.L. van der Heiden, and R. Luppes. Adaptive grid refinement for free-surface flow simulations in offshore applications. In *ASME 2015 34th International Conference on Ocean, Offshore and Arctic Engineering*, 2015.

6. Jaouen F. Bandringa H., Helder J. and Koop A. Validation of CFD for run-up and wave impact on a semi-submersible. In *International Conference on Violent Flows (VF2016), Osaka, Japan*, pages 1–10, 2016.

7. Bogdan Iwanowski, Marc Lefranc, and Rik Wemmenhove. Numerical investigation of sloshing in a tank: Statistical description of experiments and cfd calculations. In *ASME 2010 29th International Conference on Ocean, Offshore and Arctic Engineering*, pages 579–588, 2010.

8. B. Düz. *Wave Generation, Propagation and Absorption in CFD Simulations of Free Surface Flows*. PhD thesis, Delft University of Technology, 2015.